On-chip transporting arresting and characterizing individual nano-objects in biological ionic liquids

Höller, Christian ; Schnoering, Gabriel ; Eghlidi, Hadi ; Suomalainen, Maarit ; Greber, Urs F ; Poulikakos, Dimos

Abstract: Understanding and controlling the individual behavior of nanoscopic matter in liquids, the environment in which many such entities are functioning, is both inherently challenging and important to many natural and man-made applications. Here, we transport individual nano-objects, from an assembly in a biological ionic solution, through a nanochannel network and confine them in electrokinetic nanovalves, created by the collaborative effect of an applied ac electric field and a rationally engineered nanotopography, locally amplifying this field. The motion of so-confined fluorescent nano-objects is tracked, and its kinetics provides important information, enabling the determination of their particle diffusion coefficient, hydrodynamic radius, and electrical conductivity, which are elucidated for artificial polystyrene nanospheres and subsequently for sub–100-nm conjugated polymer nanoparticles and adenoviruses. The on-chip, individual nano-object resolution method presented here is a powerful approach to aid research and development in broad application areas such as medicine, chemistry, and biology.

DOI: https://doi.org/10.1126/sciadv.abd8758

On-chip transporting arresting and characterizing individual nano-objects in biological ionic liquids

Christian Höller[1], Gabriel Schnoering[1], Hadi Eghlidi[1], Maarit Suomalainen[2], Urs F. Greber[2] and Dimos Poulikakos[1]*

[1]Laboratory of Thermodynamics in Emerging Technologies, ETH Zurich, Sonneggstrasse 3, Zurich, Switzerland

[2]Department of Molecular Life Sciences, University of Zurich, Zurich, Switzerland

*Correspondence to: Dimos Poulikakos (email: dpoulikakos@ethz.ch)

Keywords
Electrokinetic forces, trapping, nanofluidics, single nanoparticle resolution, viruses, conjugated polymer nanoparticles.

Abstract

Understanding and controlling the individual behavior of nanoscopic matter in liquids, the environment in which many such entities are functioning, is both inherently challenging and important to many natural and manmade applications. Here we transport individual nano-objects, from an assembly in a biological ionic solution, through a nanochannel network and confine them in electrokinetic nanovalves, created by the collaborative effect of an applied alternating current (AC) electric field and a rationally engineered nanotopography, locally amplifying this field. The motion of so-confined fluorescent nano-objects is tracked, and its kinetics provides important information enabling the determination of their particle diffusion coefficient, hydrodynamic radius and electrical conductivity, which are elucidated for artificial polystyrene nanospheres and subsequently for sub-100 nm conjugated polymer nanoparticles and adenoviruses. The on-chip, individual nano-object resolution method presented here, is a powerful approach, to aid research and development in broad application areas such as medicine, chemistry and biology.

Introduction

Controlling the motion and determining the properties of nanoscopic objects in liquids, from synthetic to biological, is of great scientific and also practical interest in diverse fields such as biology and medicine,[1–6] nanorobotics[7,8] and chemistry.[9] As a result, a host of approaches are being developed, targeting the elusive manipulation and characterization of single nanoscale objects. These approaches often rely on the designed interaction of particles with an external force field, being fluidic,[10] optical[11–13] or electrical,[14] in order to overcome the predominant inherent thermal fluctuations.

For particles diffusing in micro- and nanochannels, electrostatic and electrokinetic approaches have been successfully implemented with charged nanoparticles in liquids at non-biological, low ionic strengths. They were used to trap, valve, or sort nano-objects of different sizes.[15–19] Working with biological particles in their natural environment, on the other hand, requires highly ionic media[20] in which electrostatic wall forces are practically shielded by the electrical double layer and restricted to short distances of just a few nanometers away from the walls.[14] In such cases, imposed electrokinetic forces have shown potential to be a major contributor in controlling the motion of a nano-object in such media and can enable their manipulation.[16,21–23]

In this work, we go well beyond kinetic control of single nano-objects in highly ionic environments, and are able to realize a directly and non-intrusively their characterization, by means of determining their important fundamental properties. We employ a pair of AC electrokinetic nanovalves in a nanochannel that are amplified by a specifically designed and fabricated channel restriction nanotopography to arrest nano-objects. The nanotopography can generate a dielectrophoretic linear restoring force on the trapped particle whose motion is then

well described by a harmonic potential. The confined kinetics of the nano-object is measured at speeds much faster than the characteristic timescale of diffusion and, in combination with theoretical analysis the particle diffusion coefficient, hydrodynamic radius and electrical conductivity are determined. In addition to known size polystyrene beads, we investigate two types of nano-objects in their native (high ionic strength) environment: adenoviruses and conjugated polymer nanoparticles (CPNs), crucial for biomedical and virology applications.

Results

Stable confinement in-between AC eletrokinetic nanovalves along the channel

Individual nanoparticles moving in biologically relevant solutions are transported and manipulated to assess their key properties. To do this, we utilize a nanofluidic channel supplemented with insulated nano-electrodes on either side of nanofabricated steps as illustrated on Fig. 1A. This combination generates a strong, controllable, electrokinetic force, when applying an AC voltage V, typically 2 V at 10 MHz. Experiments are performed in high ionic strength solutions where a dielectric particle in an AC electric field gradient is repelled from the denser region of the field. Consequently, the downstream motion of a particle is stopped by an AC electrokinetic barrier, manifesting itself through the corresponding dielectrophoretic force, which is applied at will, functioning as a switchable nanovalve.[16] Two such valves placed close together in series within the channel frame an active confinement region in between (Fig. 1A). At the starting point of an experiment, one (upstream) confining valve is open while the second (downstream) is closed. A single particle moves through the open valve and enters the confinement region (*i*). Next, the open valve is closed, and the particle is effectively trapped between the valves (*ii*). The confined dynamics of the nano-object in this location is then recorded and analyzed, which eventually enables the determination of important nano-object properties related to its motion. Finally, after characterization of the particle, the

downstream valve is opened, and the particle moves out of the confinement region (*iii*) freeing the system for the next particle.

The nanofluidic channel is carved in a silicon oxide layer at the surface of a silicon wafer. The device is fabricated with a number of steps by lithography, needed to create the desired nanotopographic features and the insulated gold electrodes placed in the nanochannels. Details of the general fabrication protocol can be found in.[16] The nanochannels and the supporting integrated circuit are placed upside down on a motorized stage on top of an inverted microscope as depicted in Fig. 1B. The channel is aligned such that the volume between two valves, where particles are confined, can be clearly imaged. Nano-objects studied in this work are fluorescent and can be excited using a blue laser diode (460 nm) focused at the back-focal plane of a high magnification oil immersion objective (100x 1.3 NA) to provide a homogeneous illumination over the confinement area. The exciting blue light is attenuated to provide a faint intensity of only 85 μW at the entrance of the objective to avoid light induced heating. The fluorescent light emitted by the particle is recollected by the objective, separated from the illumination by a dichroic mirror (cut-off at 490 nm) and a band-pass filter (500 to 600 nm) and then sent to a camera. The fluorescence signal is recorded by a fast and sensitive camera (EMCCD) at speeds up to 1000 Hz. Acquisition of the video and operation of the valves are synchronously controlled by a computer.

The dynamics of a particle in the electrokinetic valve is first illustrated by confining and recording the motion of a single fluorescent polystyrene (PS) nanosphere, with a 50 nm radius, initially in a mixture of identical beads, suspended in 0.1x phosphate-buffered saline (PBS) at room temperature $T = 294$ K, taking advantage of the sensitivity of the particle conductivity

to radio frequencies (10 MHz). We also note that Joule heating has been shown to be negligible during system operation.[16] The instantaneous position projected on the x-y plane is extracted from the recorded videos by motion tracking of the point spread function using a Gaussian filter, offering sub-pixel resolution.[24] The typical position evolution (over 10 s) of a confined particle between the valves is illustrated in Fig. 2A as a sequence of positions, each separated by 1 ms in time. The nanochannel has a width $w = 500$ nm and a height $h = 300$ nm. Above the fabricated topographic steps, the channel height is reduced to 200 nm, while the width remains the same (Fig. 2A). The space between two consecutive steps containing an electrode is $d = 600$ nm. The particle motion dynamics within the confinement volume for three different voltages V is presented in Figs. 2B and 2C, as position density histograms for displacements in the x and y directions, respectively (Fig. 2A). A clear dependence in the applied voltage is apparent for the x-motion along the channel, while the perpendicular y-motion is independent of the field strength. The position probability density in the direction of the channel axis has a Gaussian shape, which narrows significantly in going from 1.4 V to 2.2 V in applied voltage V, sharpening accordingly the imparted confinement. At 2.2 V, the deviation of the Gaussian is as small as 42 nm. The motion of the particle in the transverse y-direction experiences only the confinement exerted by the walls and the particle explores the space in this direction practically uniformly. This exploration includes direct interaction with walls characterized predominantly by short distance electrostatic forces and becomes negligible approximately 15 nm away from surfaces.[14] The position probability density uniformity is in the range ± 200 nm.

Dielectrophoretic force under AC frequency

In the following, the voltage-dependent motion along the main particle propagation x is studied, where the electric potential V imposes a direct and tunable control over the confinement of the

particle as shown in Figs. 2B and 2C and where the aim is to regulate the particle transport. The 10 MHz AC electric field applied to the electrodes generates a time-averaged field intensity $|E(x)|^2$ that acts on the confined particle. Because we are working with a high ionic strength fluid, electrostatic contributions from the channel walls are screened and have a negligible effect on the particle motion in the axial x direction of the channel. The dominant electrokinetic force is the time-averaged AC dielectrophoretic force, which for a spherical equivalent of a particle is given by[14]

$$F_{DEP}(x) = 2\pi\varepsilon_m r^3 Re[CM]\nabla|E(x)|^2, \quad [1]$$

where ε_m is the electrical permittivity of the medium, r the particle hydrodynamic radius and $Re[CM]$ the real part of their Clausius–Mossotti factor (CM). At our operating conditions, in high ionic solutions with an electric field alternating at 10 MHz, the real part of the CM factor can be written (Supporting Information S1)

$$Re[CM] = \frac{\sigma_p - \sigma_m}{\sigma_p + 2\sigma_m}, \quad [2]$$

depending only on the known medium electrical conductivity σ_m and the unknown nano-object electrical conductivity σ_p, which can hence be determined if $Re[CM]$ is obtained from the gathered kinetics data. This is achieved by designing the time-averaged AC dielectrophoretic force, $F_{DEP}(x)$, to be a linear restoring force with x, as will be discussed later.

Langevin equation of motion and linearization of AC dielectrophoretic force

The motion of the particle in the confinement space is subject to three forces and is well described by the overdamped Langevin equation. Specifically, these forces are the inherent time-dependent thermal force $F_{th}(t)$ driving the Brownian motion, the frictional fluidic drag force $F_{Drag} = -\gamma\dot{x}$, resisting motion, where γ is the time-averaged drag coefficient, and the confining dielectrophoretic force in $F_{DEP}(x)$ (Eq. 2), which yields:

$$\gamma \dot{x} = F_{DEP}(x) + F_{th}(t). \quad [3]$$

In the uncorrelated stochastic thermal force $F_{th}(t) = \sqrt{2\gamma k_B T}\Gamma(t)$, $\Gamma(t)$ is a random Gaussian process such that $< \Gamma(t) > = 0$ and $< \Gamma(t)\,\Gamma(t') > = \delta(t - t')$. We assume all studied nano-objects as spherical and of constant size over the course of the experiment. The measured drag coefficient, γ, is related to the Stokes law by $\gamma_S = \Phi\gamma$, where $\gamma_S = 6\pi\eta r$ is the Stokes drag coefficient for a freely diffusing sphere of hydrodynamic radius r in bulk water of known viscosity η and Φ is a scaling coefficient discussed in detail in (Supporting Information S2).

It is apparent from (Eqs. 2 and 3) that the overall dynamics of a nano-object subjected to the AC dielectrophoretic force $F_{DEP}(x)$ is strongly affected by the gradient of the electric field intensity $\nabla|E(x)|^2$, to which this force is proportional. Based on this, the nanochannel topography is designed and fabricated such that, while is it is geometrically simple: (*i*) it significantly increases the gradient $\nabla|E(x)|^2$ and (*ii*) it renders this gradient to be linear with respect to the displacement x in the confinement region. As shown below, the resulting linearity of the restoring force F_{DEP} provides an expression for the motion of the confined nano-object and a direct measurement of the confinement strength, the trap stiffness.

As detailed in (Supporting Information S1), the relative position and sizing of the topographic steps and electrodes are designed with the help of numerical simulations to yield a parabolic electric field intensity in the nano-object confinement region, such that $|E(x,V)|^2 = \alpha(V)^2 x^2$, with $\alpha(V)$ a proportionality coefficient that only depends on the applied potential V and the geometry of the channel. The gradient of the square of the field intensity is therefore linear and reads $\nabla|E(x,V)|^2 = 2\alpha(V)^2 x$. The coefficient $\alpha(V)$ is shown by the numerical simulation (Supporting Information S1) to be linear with respect to the applied voltage V and $\alpha(V) = \beta V$, where $\beta = 1062.3 \times 10^9$ m^{-2} is a topography-dependent, geometric coefficient determined

numerically in the dipole limit.[25] Based on the above, (Eq. 2) can be written $F_{DEP}(x) = -\kappa(V)x$ where the voltage-dependent trap stiffness is

$$\kappa(V) = -4\pi\varepsilon_m r^3 Re[CM]\beta^2 V^2. \quad [4]$$

Spectral analysis of the confined motion

The measured time evolution of the motion of a confined particle along x in its confinement space is presented on Fig. 3A. The video tracking is calibrated by imaging the known distance between electrodes of the nanochannel and therefore all extracted positions express themselves directly in meters. The graph depicts the successive positions of a confined 100 nm polystyrene bead over 10 s with motional noise distributed around a constant mean value, typical for Brownian motion under the influence of a linear restoring force. To properly characterize the dynamics, the self-similar nature of the Brownian motion is exploited by examining its autocorrelation. This correlation is readily obtained from the power spectral density (PSD), which is the modulus of the displacement frequency of the particle squared. In the case of the Langevin equation (Eq. 3), the PSD is a Lorentzian (see Supporting Information S3) function and reads:[26]

$$P_{xx}(f) = \frac{D}{2\pi^2(f_T^2+f^2)}, \quad [5]$$

where $D = \frac{k_B T}{\gamma}$ is the diffusion coefficient and $f_T = \frac{\kappa(V)}{2\pi\gamma}$ is the roll-off value of the motion frequency f. The PSD is parametrized only by the diffusion coefficient D and the roll-off frequency f_T, determined by fitting the experimental data based on the above expression. This enables the determination of the drag coefficient γ and the trap stiffness $\kappa(V)$ resulting by the DEP force, quantifying the strength of the confinement. A maximum likelihood estimation of $P_{xx}(f)$ is performed on the experimental spectral density to obtain D and f_T.[27] The fitted PSD

is corrected for low-pass filtering effects from the detection instrumentation and distortions from aliasing, which are negligible in our case.[28]

Spectral densities for the x-motion are presented in Fig. 3B for a set of amplitudes V ($V = 1.4$ V, $V = 1.8$ V and $V = 2.2$ V) and nicely follow the Lorentzian shape of (Eq. 5), as shown by the fitting curves (black lines). The position noise detection limit, shown in gray, is two orders of magnitude lower than the displacement signal at low frequencies. The resulting position resolution extracted from the noise measurement is below 10 nm. Roll-off frequencies f_T are around tens of Hz and increase with the electric field amplitude. Our setup, recording the motion at 1000 Hz, is well capable of measuring the two characteristic regimes of the PSD. At low frequencies ($f^2 \ll f_T^2$), a frequency independent plateau is observed with value $\frac{D}{2\pi^2 f_T^2}$ that characterizes the confined motion of the nanoparticle. Steady-state throughout the acquisition is verified from the displacements of the nano-objects at low frequencies strictly following the expected plateau value. In the high frequency region ($f^2 \gg f_T^2$), the confinement is not effective anymore and free diffusion occurs. The spectral density becomes $\frac{D}{2\pi^2 f^2}$ and follows a f^{-2} decrease proportional to the diffusion coefficient. It is worth noting that the PSD for the y-motion perpendicular to the channel, shown in Fig. 3C, displays no dependency on the electrokinetic forces and imposed voltages in its spectral signatures, as expected given the absence of imposed electric field in this direction.

Measurement of the particle hydrodynamic radius

The knowledge of the diffusion coefficient D makes possible the direct determination of the drag coefficient γ in the confinement region, as mentioned earlier. The drag force has a strong dependence on the viscosity of the fluid. In our experiments, the viscosity does not change with

the ionic strength. However, due to the tight nanochannel dimensions, the particle motion reaches the close vicinity of the walls. Specifically, the particle is enclosed inside the four channel walls, which have an impact on the fluid flow generated by the moving particle and therefore affect the associated drag force. The measured drag coefficient, γ, needs to be related to the Stokes drag coefficient for freely diffusing particles in water, γ_S, in order to be able to obtain the particle hydrodynamic radius, as mentioned earlier.[29–31] The introduced scaling factor Φ is parametrized by the yet unknown hydrodynamic radius r of the particle. While corrections to the drag are readily available in the absence of external forces for a particle of a known radius at a fixed position with respect to an interface,[32,33] the particle in our case moves and explores most of the confinement volume during measurements. Electrokinetic forces also influence the particle vertical position in the z direction. The measured drag coefficient, γ, represents the normalized averaged mobility of the particle in its energy landscape,[34] which accounts for the impermeable boundaries of the nanochannel as well as the electrostatic[35] and electrokinetic[16,36] interactions with the particle. The drag force and Φ can be obtained numerically[32] (Supporting Information S2). This provides a direct path for the determination of hydrodynamic radius r of the nano-object, $r = \Phi\gamma/(6\pi\eta)$.

With knowledge of the drag coefficient γ and the roll-off frequency f_T, extracted from the PSD, the trap stiffness $\kappa(V) = 2\pi\gamma f_T$ is obtained. Time traces are systematically acquired for a large number of confined PS beads with varying applied voltages V, from which the trap stiffness κ and the hydrodynamics radius r are both determined and presented on Fig. 4, panels A and B respectively. The dielectrophoretic force effecting the confinement is tuned by adjusting the potential amplitude V, as seen in Fig. 3B, resulting in varying roll-off frequencies f_T and therefore a varying trap stiffness $\kappa(V)$. A systematic study of this variation is reported in Fig. 4A and shows the evolution of the trap stiffness for PS beads (in blue) with the applied voltage

V in the range from 1.3 to 2.2 V by steps of 0.1 V. For example, the trap stiffness κ for 100 nm PS beads under an applied potential of 2 V is $\kappa = 0.85$ pN/μm. Our trap stiffnesses are comparable to those obtained using plasmonic tweezers[37,38] but they are lower than reported values for electrostatic trapping of metallic spheres of similar sizes for very low ionic strengths ($< 10^{-1}$ mM).[15,39]

Measured hydrodynamic radii (Fig. 4B, blue points) are found to be independent of the electric field amplitude V and average to $r = 51.3 \pm 12.4$ nm between 1.3 and 2 V, which is in good agreement with manufacturer values ($r = 50 \pm 3.15$ nm) and our own verification measurements (SEM images where $r = 50.9 \pm 4.3$ nm, see Supporting Information S4). All error bars represent the experimental uncertainties at a 95% confidence interval (2 standard deviations) for a collection of particles measured at a given voltage V.

Measurement of the particle conductivity

The force $F_{DEP}(x, V)$ exerted on the particle depends on the position x of the particle and the applied electric voltage V. As mentioned earlier, with the help of numerical simulations (Supporting Information S1) the nanovalve topography is designed such that the dielectrophoretic force in the confinement region is linear in the x direction and the trap stiffness is proportional to the square of the applied potential V (Eq. 4). For PS beads this is confirmed in Fig. 4A, where the trap stiffness exhibits a quadratic behavior (best fit in blue line) with respect to V. Data points at 1.3 V and above 2 V depart slightly from this trend. Low voltages allow the beads to explore a wider confinement space, sometimes partially escaping and then returning to the center of the confinement region. On the contrary, beads trapped at high voltages are so tightly confined that their PSD motion approaches the detection limit noise, in particular at high frequencies. As the background noise contributes to the overall signal

amplitude, estimation of dynamical parameters becomes biased. This is clearly apparent in Fig. 3B for $V = 2.2$ V, where the roll-off frequency is $f_T = 80$ Hz. At this frequency, the background noise contributes already one tenth of the PSD rendering a proper estimation in the high frequency region difficult. Therefore, experiments at low and high V define the limits of validity for our approach, i.e. the bounds of the region where the dielectrophoretic force is linear and significantly over the motion noise, allowing a reliable determination of the nano-objects properties.

With a chosen applied electric potential V and an already determined hydrodynamic radius r, the measured trap stiffness $\kappa(V)$, (Eq. 4), only depends on the real part of the CM factor, $Re[CM]$, which can thus be determined. This also yields the particle conductivity $\sigma_p = \frac{\sigma_m(2Re[CM]+1)}{1-Re[CM]}$ from (Eq. 1), with the ionic strength of the solution set at a medium conductivity of $\sigma_m = 0.24$ S/m. The conductivity of the 100 nm PS beads (in 0.1x PBS) is shown in Fig. 4B (red points) for different voltages. It is, as expected, found to be voltage independent, and has a mean value $\sigma_p = 0.15 \pm 0.04$ S/m.

By studying known property polystyrene nanospheres, we have shown that a careful analysis of the confined particle motion dynamics, results in the determination of a host of important particle properties. Next, we venture into unknown property nano-objects, relevant to biological applications, namely conjugated polymer nanoparticles (CPNs) and adenoviruses and target the determination of the same properties.

Characterization of conjugated polymer nanoparticles and adenoviruses

CPNs are a family of macromolecules with large delocalized π-conjugated backbones. Compared to quantum dots, they show lower cytotoxicity, high photostability, high fluorescence and no blinking,[40–43] making them favorable for a variety of biological applications. Their strong opto-electronic performances[42,44] and fluorescence allow them to be used for combined diagnostics and treatment, in theranostics applications.[44,45] Manipulation and characterization of CPNs at the single entity level has not been yet reported, to the best of our knowledge. Furthermore, we study adenoviruses. They are common pathogens in humans and animals. The ability to control and study them individually and can help in the challenging determination of their infection pathway.[46,47]

The CPNs are found to be well confined by the electrokinetic forces, similar to PS beads, even though their fluorescence is weaker. The roll-off frequencies, diffusion coefficients are measured from PSDs (Supporting Information S5) as needed to determine the CPNs hydrodynamic radius and electrical conductivity, which are presented in Fig. 4C for varying electric voltages. The measurements are voltage invariant and the mean values are estimated from all measurements between 1.3 to 2.0 V. The confinement of CPNs has a typical trap stiffnesses of $\kappa = 0.48$ pN/μm at 2 V. The CPN hydrodynamic radius averages to $r = 45 \pm 11.7$ nm while their electrical conductivity has a value of $\sigma_p = 0.14 \pm 0.06$ S/m. The CPN suspension is relatively homogeneous with respect to particle size and the dispersion around the mean is small. This makes these particles practically suited for controlled applications in biological environments such as drug delivery in small capillaries and light activated local heating.

The adenoviruses (AdV-TS1) are grown in-vitro and are doped with a fluorescent dye (Alexa Fluor 488 5-TFP amine reactive dye). The viruses are trapped and investigated for voltage

amplitudes between 1.25 and 1.9 V. The confinement of the viruses is found to be stable (Supplementary Information S5), with a typical trap stiffness of $\kappa = 0.2$ pN/μm at 1.9 V. One measurement (for each electrical potential) could be performed per virus, before the fluorescence signal decreases due to particle bleaching, which hinders further detection. Spectral densities were computed from time traces recorded at 500 Hz, resulting in a measured mean hydrodynamic radius of $r = 36.1 \pm 7.1$ nm and a mean electrical conductivity of $\sigma_p = 0.15 \pm 0.04$ S/m. While the determined measurement values and error bars for viruses are reasonable throughout our experiments, the statistics of these particular experiments is somewhat limited compared to PS beads and CPNs, averaging to 10 data points per voltage.

The measured in-situ hydrodynamic radius is in good agreement with size measurements of similar adenoviruses but in a different environment, using electron microscopy.[48,49] Conductivity measurements of the individual viruses are also comparable to average values obtained for other viruses with ensemble measurements. Values for the conductivity of larger (200 nm) herpes simplex viruses, at lower ionic concentrations, are reported to be 0.1 S/m.[50] The tobacco mosaic virus has a rod shape (length of 280 nm for a width of only 18 nm) and a reported larger conductivity of 0.4 S/m.[51] The adenoviruses and previously uncharacterized synthetic conjugated polymer nanoparticles of the present work are found to have limited size disparity. Our experimental approach can be very useful in determining size and related property disparity with single entity resolution, not amenable to ensemble methods, but important to biological bio-objects, in our quest to understand mechanisms of processes such as infectivity.[46]

Discussion

We have shown that the on-chip, rational design of an electrokinetic nanovalve system with a linearly restoring trapping mechanism, combined with the analysis of the resulting, judiciously restricted, particle motion dynamics, enables the determination, within seconds, of a host of important properties of dielectric and biological nano-objects smaller than a hundred nanometers, at biological level ionic concentrations. Polystyrene beads, as well as unknown property biological nanoparticles (CPNs and adenoviruses) are controlled and characterized at the individual particle level. The present platform is a significant advancement supplementing existing approaches, such as optical spectroscopy,[52] aiming at advancing fundamental knowledge and applications involving a broad range of nanoscale matter operating in liquids.

Methods

Preparation of biological and synthetic particles

Carboxylated polystyrene beads of mean diameter 100 ± 6.3 nm from ThermoFisher (FluoSpheres, F8803) are used for the experiments. The beads are loaded with a proprietary dye, a fluorescent molecule with an absorption peak at 505 nm and an emission peak at 515 nm. The initial concentration of 2% solids was diluted 1:200 to obtain a 0.1x phosphate buffered saline concentration (PBS, Gibco).

Conjugate-polymer nanoparticles (CPN 510, Stream Bio) with an advertised hydrodynamic radius of 80 nm are also used. The particles exhibit an emission peak at 510 nm with an absorption peak at 450 nm. The initial concentration of 0.1 mg/mL was diluted 1:100 with buffered saline (PBS, Gibco) and di-ionized water to achieve a 0.1x buffer concentration.

Solution of adenoviruses, HAdV-C2_TS1 were prepared the same way as previously reported.[16] The particles exhibit an emission peak at 525 nm with an absorption peak at 488 nm. The solution was diluted with phosphate buffered saline (PBS, Gibco), Bovine Serum Albumin (BSA, Sigma Aldrich) and di-ionized water, to achieve a solution with 0.1x PBS and 5wt% BSA concentration.

Data availability

Relevant data supporting the findings of this study are available from the corresponding authors upon request.

References

(1) Pang, Y.; Song, H.; Kim, J. H.; Hou, X.; Cheng, W. Optical Trapping of Individual Human Immunodeficiency Viruses in Culture Fluid Reveals Heterogeneity with Single-Molecule Resolution. *Nat. Nanotechnol.* **2014**, *9* (8), 624–630. https://doi.org/10.1038/nnano.2014.140.

(2) Greber, U. F.; Way, M. A Superhighway to Virus Infection. *Cell* **2006**, *124* (4), 741–754. https://doi.org/10.1016/j.cell.2006.02.018.

(3) Cho, K.; Wang, X.; Nie, S.; Chen, Z.; Shin, D. M. Therapeutic Nanoparticles for Drug Delivery in Cancer. *Clin. Cancer Res.* **2008**, *14* (5), 1310–1316. https://doi.org/10.1158/1078-0432.CCR-07-1441.

(4) Amstad, E.; Reimhult, E. Nanoparticle Actuated Hollow Drug Delivery Vehicles. *Nanomedicine* **2011**, *7* (1), 145–164. https://doi.org/10.2217/nnm.11.167.

(5) Aguilar, C. A.; Craighead, H. G. Micro- and Nanoscale Devices for the Investigation of Epigenetics and Chromatin Dynamics. *Nat. Nanotechnol.* **2013**, *8* (10), 709–718. https://doi.org/10.1038/nnano.2013.195.

(6) Kumar, C. S. S. R. *Nanotechnology Characterization Tools for Biosensing and Medical Diagnosis*; 2018. https://doi.org/10.1007/978-3-662-56333-5.

(7) Li, J.; Ávila, B. E. F. De; Gao, W.; Zhang, L.; Wang, J. Micro/Nanorobots for Biomedicine: Delivery, Surgery, Sensing, and Detoxification. *Sci. Robot.* **2017**, *2* (4), 1–10. https://doi.org/10.1126/scirobotics.aam6431.

(8) Ghosh, A.; Fischer, P. Controlled Propulsion of Artificial Magnetic Nanostructured Propellers. *Nano Lett.* **2009**, *9* (6), 2243–2245. https://doi.org/10.1021/nl900186w.

(9) Daniel, M. C.; Astruc, D. Gold Nanoparticles: Assembly, Supramolecular Chemistry, Quantum-Size-Related Properties, and Applications Toward Biology, Catalysis, and Nanotechnology. *Chem. Rev.* **2004**, *104* (1), 293–346. https://doi.org/10.1021/cr030698+.

(10) Wunsch, B. H.; Smith, J. T.; Gifford, S. M.; Wang, C.; Brink, M.; Bruce, R. L.; Austin, R. H.; Stolovitzky, G.; Astier, Y. Nanoscale Lateral Displacement Arrays for the Separation of Exosomes and Colloids down to 20nm. *Nat. Nanotechnol.* **2016**, *11* (11), 936–940. https://doi.org/10.1038/nnano.2016.134.

(11) Wu, W.; Zhu, X.; Zuo, Y.; Liang, L.; Zhang, S.; Zhang, X.; Yang, Y. Precise Sorting of Gold Nanoparticles in a Flowing System. *ACS Photonics* **2016**, *3* (12), 2497–2504. https://doi.org/10.1021/acsphotonics.6b00737.

(12) Cuche, A.; Canaguier-Durand, A.; Devaux, E.; Hutchison, J. A.; Genet, C.; Ebbesen, T. W. Sorting Nanoparticles with Intertwined Plasmonic and Thermo-Hydrodynamical Forces. *Nano Lett.* **2013**, *13* (9), 4230–4235. https://doi.org/10.1021/nl401922p.

(13) Tkachenko, G.; Brasselet, E. Optofluidic Sorting of Material Chirality by Chiral Light. *Nat. Commun.* **2014**, *5*, 1–7. https://doi.org/10.1038/ncomms4577.

(14) Morgan, H.; Green, N. G. *AC Electrokinetics: Colloids and Nanoparticles*; Research Studies Press: Philadelphia, PA, 2003.

(15) Krishnan, M.; Mojarad, N.; Kukura, P.; Sandoghdar, V. Geometry-Induced Electrostatic Trapping of Nanometric Objects in a Fluid. *Nature* **2010**, *467* (7316), 692–695.

(16) Eberle, P.; Höller, C.; Müller, P.; Suomalainen, M.; Greber, U. F.; Eghlidi, H.;

Poulikakos, D. Single Entity Resolution Valving of Nanoscopic Species in Liquids. *Nat. Nanotechnol.* **2018**, *13* (7), 578–582. https://doi.org/10.1038/s41565-018-0150-y.

(17) Skaug, M. J.; Schwemmer, C.; Fringes, S.; Rawlings, C. D.; Knoll, A. W. Nanofluidic Rocking Brownian Motors. *Science (80-.).* **2018**, *359* (6383), 1505–1508. https://doi.org/10.1126/science.aal3271.

(18) Mojarad, N.; Sandoghdar, V.; Krishnan, M. Measuring Three-Dimensional Interaction Potentials Using Optical Interference. *Opt. Express* **2013**, *21* (8), 9377–9389. https://doi.org/10.1364/OE.21.009377.

(19) Ruggeri, F.; Zosel, F.; Mutter, N.; Rozycka, M.; Wojtas, M.; Ozyhar, A.; Schuler, B.; Krishnan, M. Single-Molecule Electrometry. *Nat. Nanotechnol.* **2017**, *12* (5), 488–495. https://doi.org/10.1038/nnano.2017.26.

(20) Williams, R. J. P. *The Natural Selection of the Chemical Elements*; Clarendon Press: New York, 1997; Vol. 53. https://doi.org/10.1007/s000180050102.

(21) Morgan, H.; Hughes, M. P.; Green, N. G. Separation of Submicron Bioparticles by Dielectrophoresis. *Biophys. J.* **1999**, *77* (1), 516–525. https://doi.org/10.1016/S0006-3495(99)76908-0.

(22) Barik, A.; Zhang, Y.; Grassi, R.; Nadappuram, B. P.; Edel, J. B.; Low, T.; Koester, S. J.; Oh, S. H. Graphene-Edge Dielectrophoretic Tweezers for Trapping of Biomolecules. *Nat. Commun.* **2017**, *8* (1). https://doi.org/10.1038/s41467-017-01635-9.

(23) Cohen, A. E.; Moerner, W. E. Suppressing Brownian Motion of Individual Biomolecules in Solution. *Proc. Natl. Acad. Sci. U. S. A.* **2006**, *103* (12), 4362–4365. https://doi.org/10.1073/pnas.0509976103.

(24) Aguet, F.; Antonescu, C. N.; Mettlen, M.; Schmid, S. L.; Danuser, G. Advances in Analysis of Low Signal-to-Noise Images Link Dynamin and AP2 to the Functions of an Endocytic Checkpoint. *Dev. Cell* **2013**, *26* (3), 279–291. https://doi.org/10.1016/j.devcel.2013.06.019.

(25) Washizu, M.; Jones, T. B. Generalized Multipolar Dielectrophoretic Force and Electrorotational Torque Calculation. *J. Electrostat.* **1996**. https://doi.org/10.1016/S0304-3886(96)00025-3.

(26) Berg-Sørensen, K.; Flyvbjerg, H. Power Spectrum Analysis for Optical Tweezers. *Rev. Sci. Instrum.* **2004**, *75* (3), 594–612. https://doi.org/10.1063/1.1645654.

(27) Nørrelykke, S. F.; Flyvbjerg, H. Power Spectrum Analysis with Least-Squares Fitting: Amplitude Bias and Its Elimination, with Application to Optical Tweezers and Atomic Force Microscope Cantilevers. *Rev. Sci. Instrum.* **2010**, *81* (7). https://doi.org/10.1063/1.3455217.

(28) Lansdorp, B. M.; Saleh, O. A. Power Spectrum and Allan Variance Methods for Calibrating Single-Molecule Video-Tracking Instruments. *Rev. Sci. Instrum.* **2012**, *83* (2). https://doi.org/10.1063/1.3687431.

(29) Leach, J.; Mushfique, H.; Keen, S.; Di Leonardo, R.; Ruocco, G.; Cooper, J. M.; Padgett, M. J. Comparison of Faxén's Correction for a Microsphere Translating or Rotating near a Surface. *Phys. Rev. E - Stat. Nonlinear, Soft Matter Phys.* **2009**, *79* (2), 1–4. https://doi.org/10.1103/PhysRevE.79.026301.

(30) Goldman, A. J.; Cox, R. G.; Brenner, H. Slow Viscous Motion of a Sphere Parallel to a Plane Wall-II Couette Flow. *Chem. Eng. Sci.* **1967**, *22* (4), 653–660.

https://doi.org/10.1016/0009-2509(67)80048-4.

(31) Faxen, H. Die Bewegung Einer Starren Kugel Langs Der Achse Eines Mit Zaher Flussigkeit Gefullten Rohres. *Ark. Matemetik Astron. och Fys.* **1923**, *17*, 1–28.

(32) Feitosa, M. I. M.; Mesquita, O. N. Wall-Drag Effect on Diffusion of Colloidal Particles near Surfaces: A Photon Correlation Study. *Phys. Rev. A* **1991**, *44* (10), 6677–6685. https://doi.org/10.1103/PhysRevA.44.6677.

(33) Fringes, S.; Holzner, F.; Knoll, A. W. The Nanofluidic Confinement Apparatus: Studying Confinement-Dependent Nanoparticle Behavior and Diffusion. *Beilstein J. Nanotechnol.* **2018**, *9* (1), 301–310. https://doi.org/10.3762/bjnano.9.30.

(34) Pawar, Y.; Anderson, J. L. Hindered Diffusion in Slit Pores: An Analytical Result. *Ind. Eng. Chem. Res.* **1993**, *32* (4), 743–746. https://doi.org/10.1021/ie00016a023.

(35) Das, P. K.; Bhattacharjee, S. Electrostatic Double Layer Force between a Sphere and a Planar Substrate in the Presence of Previously Deposited Spherical Particles. *Langmuir* **2005**, *21* (10), 4755–4764. https://doi.org/10.1021/la047147e.

(36) Pethig, R. Electrical Potential Energy and Electric Potential. In *Dielectrophoresis*; John Wiley & Sons, Ltd, 2017; pp 77–91. https://doi.org/10.1002/9781118671443.ch4.

(37) Volpe, G.; Quidant, R.; Badenes, G.; Petrov, D. Surface Plasmon Radiation Forces. *Phys. Rev. Lett.* **2006**, *96* (23), 1–4. https://doi.org/10.1103/PhysRevLett.96.238101.

(38) Grigorenko, A. N.; Roberts, N. W.; Dickinson, M. R.; Zhang, Y. Nanometric Optical Tweezers Based on Nanostructured Substrates. *Nat. Photonics* **2008**, *2* (6), 365–370. https://doi.org/10.1038/nphoton.2008.78.

(39) Celebrano, M.; Rosman, C.; Sönnichsen, C.; Krishnan, M. Angular Trapping of Anisometric Nano-Objects in a Fluid. *Nano Lett.* **2012**, *12* (11), 5791–5796. https://doi.org/10.1021/nl303099c.

(40) Efros, A. L.; Nesbitt, D. J. Origin and Control of Blinking in Quantum Dots. *Nature Nanotechnology*. Nature Publishing Group 2016, pp 661–671. https://doi.org/10.1038/nnano.2016.140.

(41) Braeken, Y.; Cheruku, S.; Ethirajan, A.; Maes, W. Conjugated Polymer Nanoparticles for Bioimaging. *Materials (Basel).* **2017**, *10* (12), 1–23. https://doi.org/10.3390/ma10121420.

(42) Abelha, T. F.; Phillips, T. W.; Bannock, J. H.; Nightingale, A. M.; Dreiss, C. A.; Kemal, E.; Urbano, L.; Demello, J. C.; Green, M.; Dailey, L. A. Bright Conjugated Polymer Nanoparticles Containing a Biodegradable Shell Produced at High Yields and with Tuneable Optical Properties by a Scalable Microfluidic Device. *Nanoscale* **2017**, *9* (5), 2009–2019. https://doi.org/10.1039/c6nr09162h.

(43) Feng, L.; Zhu, C.; Yuan, H.; Liu, L.; Lv, F.; Wang, S. Conjugated Polymer Nanoparticles: Preparation, Properties, Functionalization and Biological Applications. *Chem. Soc. Rev.* **2013**, *42* (16), 6620–6633. https://doi.org/10.1039/c3cs60036j.

(44) Qian, C. G.; Chen, Y. L.; Feng, P. J.; Xiao, X. Z.; Dong, M.; Yu, J. C.; Hu, Q. Y.; Shen, Q. D.; Gu, Z. Conjugated Polymer Nanomaterials for Theranostics. *Acta Pharmacol. Sin.* **2017**, *38* (6), 764–781. https://doi.org/10.1038/aps.2017.42.

(45) Wang, Y.; Feng, L.; Wang, S. Conjugated Polymer Nanoparticles for Imaging, Cell Activity Regulation, and Therapy. *Adv. Funct. Mater.* **2019**, *29* (5), 1–20.

https://doi.org/10.1002/adfm.201806818.

(46) Seisenberger, G.; Ried, M. U.; Endress, T.; Büning, H.; Hallek, M.; Bräuchle, C. Real-Time Single-Molecule Imaging of the Infection Pathway of an Adeno-Associated Virus. *Science* **2001**, *294* (October), 1929–1932. https://doi.org/10.1126/science.1064103.

(47) Lakadamyali, M.; Rust, M. J.; Babcock, H. P.; Zhuang, X. Visualizing Infection of Individual Influenza Viruses. *Proc. Natl. Acad. Sci. U. S. A.* **2003**, *100* (16), 9280–9285. https://doi.org/10.1073/pnas.0832269100.

(48) Reddy, V. S.; Natchiar, S. K.; Stewart, P. L.; Nemerow, G. R. Crystal Structure of Human Adenovirus at 3.5 A Resolution. *Science (80-.).* **2010**, *329* (5995), 1071–1075.

(49) Liu, H.; Jin, L.; Koh, S. B. S.; Atanasov, I.; Schein, S.; Wu, L.; Zhou, Z. H. Atomic Structure of Human Adenovirus by Cryo-EM Reveals Interactions Among Protein Networks. *Science (80-.).* **2010**, *329* (5995), 1038 LP – 1043. https://doi.org/10.1126/science.1187433.

(50) Hughes, M. P.; Morgan, H.; Rixon, F. J. Measuring the Dielectric Properties of Herpes Simplex Virus Type 1 Virions with Dielectrophoresis. *Biochim. Biophys. Acta - Gen. Subj.* **2002**, *1571* (1), 1–8. https://doi.org/10.1016/S0304-4165(02)00161-7.

(51) Ermolina, I.; Morgan, H.; Green, N. G.; Milner, J. J.; Feldman, Y. Dielectric Spectroscopy of Tobacco Mosaic Virus. *Biochim. Biophys. Acta - Gen. Subj.* **2003**, *1622* (1), 57–63. https://doi.org/10.1016/S0304-4165(03)00118-1.

(52) Squires, A. H.; Dahlberg, P. D.; Liu, H.; Magdaong, N. C. M.; Blankenship, R. E.; Moerner, W. E. Single-Molecule Trapping and Spectroscopy Reveals Photophysical

Heterogeneity of Phycobilisomes Quenched by Orange Carotenoid Protein. *Nat. Commun.* **2019**, *10* (1). https://doi.org/10.1038/s41467-019-09084-2.

Acknowledgements

The work was supported partially by the Swiss National Foundation under grant 200021_162855, and Swiss National Foundation grant number 31003A_179256 / 1.

Associated Content

Supporting Information

Figures S1-S3 present the design of the AC-dielectrophoretic force profile and its structural characterization; Figures S4-S5 present the correction to the drag for the confined motion inside the trap and the determination of the hydrodynamic radius; Derivation of the spectral density for the overdamped Langevin equation with a linear restoring force; Figure S6 shows the size distribution from SEM measurements for the polystyrene microspheres

Author Information

Corresponding Author

Dimos Poulikakos - Laboratory of Thermodynamics in Emerging Technologies, ETH Zurich CH-8092 Zurich, Switzerland; orcid.org/0000-0001-5733-6478; Email: dpoulikakos@ethz.ch

Authors

Christian Höller − Laboratory of Thermodynamics in Emerging Technologies, ETH Zurich CH-8092 Zurich, Switzerland;

Gabriel Schnoering − Laboratory of Thermodynamics in Emerging Technologies, ETH Zurich CH-8092 Zurich, Switzerland; orcid.org/0000-0002-9231-9021

Hadi Eghlidi − Laboratory of Thermodynamics in Emerging Technologies, ETH Zurich CH-8092 Zurich, Switzerland; orcid.org/0000-0002-0671-3111

Maarit Suomalainen − Institute of Molecular Life Sciences, University of Zurich, Zurich, Switzerland; orcid.org/0000-0002-3276-3008

Urs F. Greber − Institute of Molecular Life Sciences, University of Zurich, Zurich, Switzerland; orcid.org/0000-0003-2278-120X

Competing interests

The authors declare no competing financial interests.

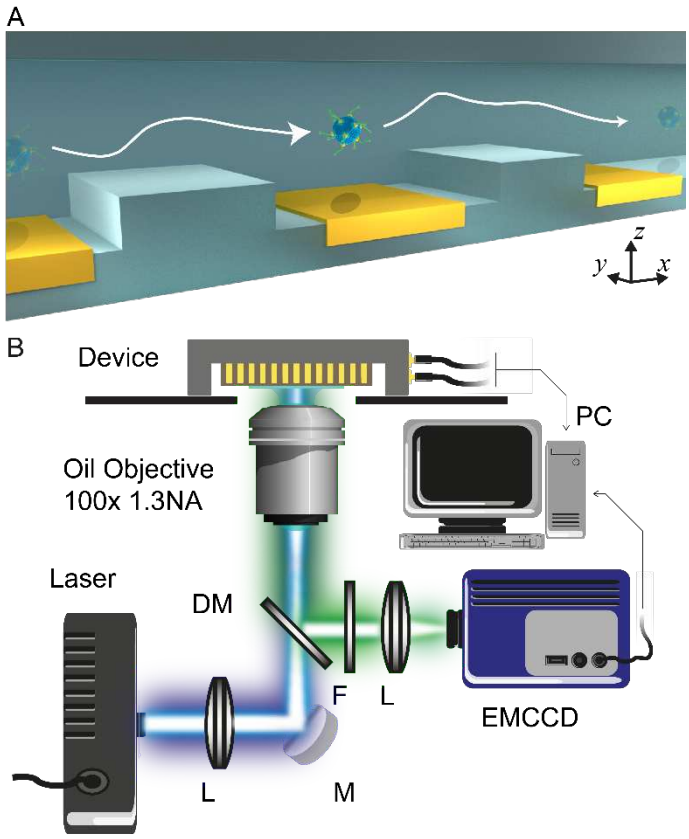

Figure 1. Electrokinetic valves experimental setup. (A) Schematic of the electrokinetic nanovalve system that enables the confinement and measurement of single nano-objects. The 300 nm high and 500 nm wide nanochannel allows the generation of a dielectrophoretic force between the electrodes when driven by an AC potential. A 100 nm high dielectric step between the electrodes increases the electric field locally and amplifies the force exerted on a particle in the nanochannel. This creates an impenetrable barrier for the particle. The barrier can be selectively opened or closed, depending on the presence of the electric potential between the electrodes. Placing two such valves close to each other creates a confinement zone on top of the electrode shared by both valves. The controlled confinement and release of particles, here illustrated by a virus drawing, is performed by opening and closing the valves. (B) The motion of the particle is recorded by a fast and sensitive camera (Andor iXon Ultra 888). The camera records the fluorescence emitted by the particle, which is excited by a blue laser (laser diode, 460 nm, 1600 mW). The blue light is focused with a lens (L) at the back-focal plane of an oil immersion objective (Olympus 100x, 1.3 NA) illuminating homogeneously the confinement volume. Light emitted by the particle is collected by the objective, separated from illumination by a dichroic mirror (DM) and a bandpass filter (F) and then sent to the camera. Acquisition of the video and operation of the valves are synchronously controlled by a computer.

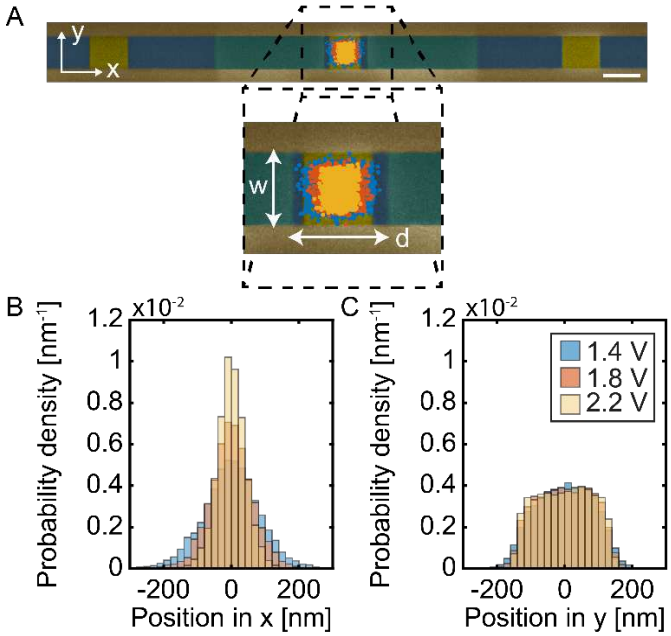

Figure 2. Recorded positions and statistics of a confined 100 nm polysterene sphere in the nanochannel. (A) False-colored SEM image of the nanochannel with the recorded measured position of a 100 nm polystyrene bead superimposed. The bottom of the channel is depicted in dark blue and the side walls, at a distance of $w = 500$ nm, in brown. Three electrodes, forming two valves, are shown in gold color and the two fabricated steps, separated by $d = 600$ nm, on each side of the central electrode in green. Successive positions (recorded for 10 s at 1000 Hz) of a confined polystyrene sphere are overlaid, for DEP potentials of 2.2 V (yellow), 1.8 V (red) and 1.4 V (blue), respectively. The white scale bar is 500 nm. Panels (B) and (C) show the position probability density in the axial (x axis) and transverse (y axis) channel directions. The position probability density in the axial direction of the channel has a Gaussian shape and becomes narrower with increasing AC potentials. In the transverse direction the particle only experiences the confinement of the walls and therefore explores uniformly the space.

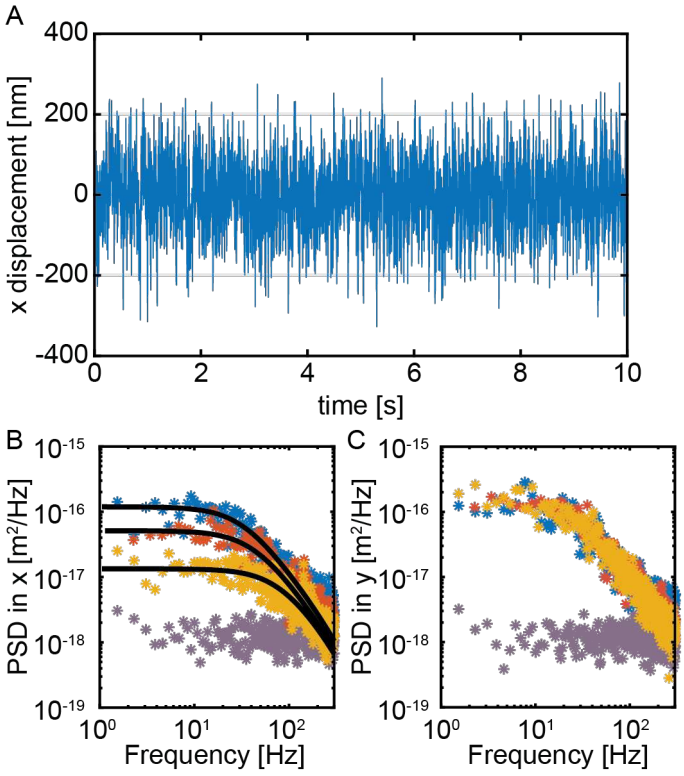

Figure 3. Study of the motion dynamics of a confined particle: (A) Position evolution of the center-of-mass of the PS bead shown in figure 2, in the axial direction of the channel, for an electrode potential of 1.4 V. The DEP force limits the motion of the bead in-between the two valves. The time-trace exhibits the typical dynamics of a confined Brownian particle. The power spectral density (PSD) is shown on panels (B) and (C) for axial displacements, along the x axis and transverse displacements, along the y axis of the channel, respectively. PSDs are shown for potentials 1.4 V (blue), 1.8 V (red) and 2.2 V (yellow) and correspond to experiments shown on Fig. 2. The spectral noise floor (grey) is determined by analysing the apparent displacements of an immobile PS bead on the glass ceiling over the confinement volume (electrodes off). PSDs are acquired at 1000 Hz and averaged 8 times to improve readability. As shown in panel (B), the x-dynamics follow a Lorentzian shape (fit in black lines) as expected for harmonic potentials. Similarly, with the histograms in figure 2, the motion varies with the DEP potential strengths. The roll-off frequency f_T and therefore the confinement stiffness increases with the applied voltage ($f_T = 33$ Hz for 1.4 V, $f_T = 43$ Hz for 1.8 V and $f_T = 80$ Hz for 2.2 V). As shown in panel (C), the y-dynamics is invariant to the external potential.

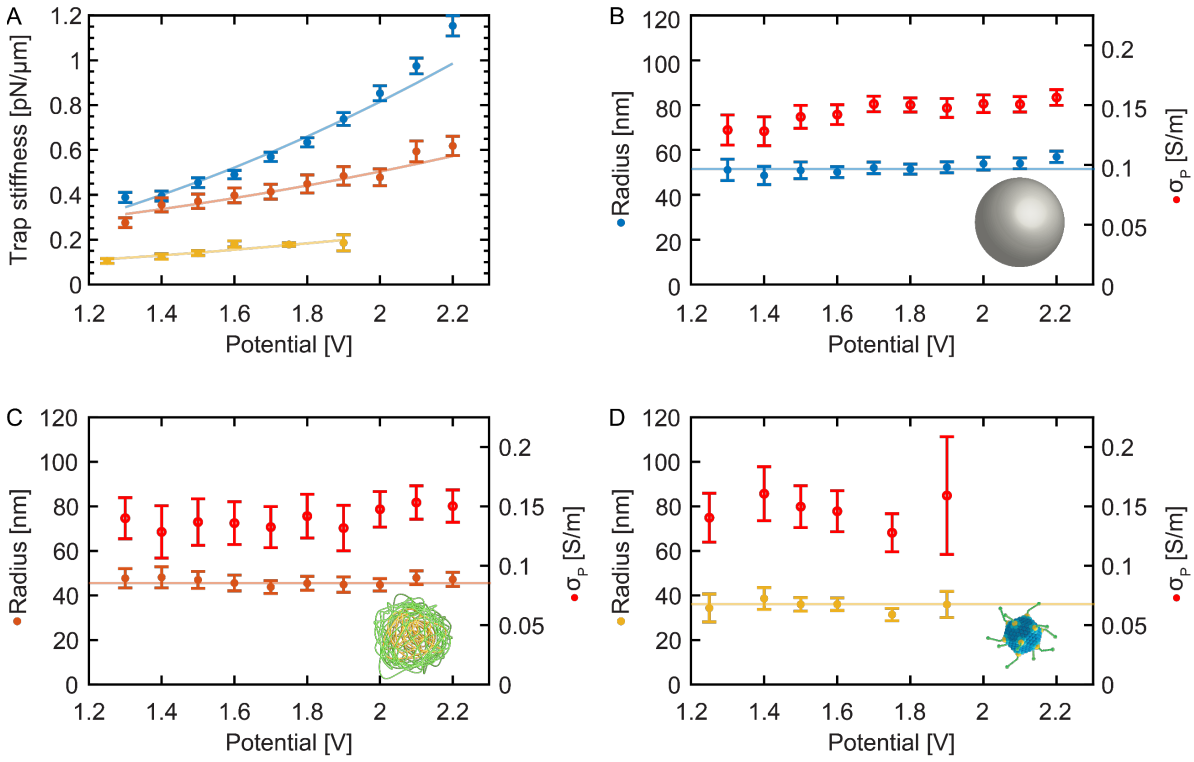

Figure 4. Confinement stiffness, hydrodynamic radius and conductivity. (A) The trap stiffness $\kappa(V)$ along the channel x axis of the measured 50 nm radius PS beads (blue points), CPNs (orange points) and adenoviruses (yellow points) is shown as a function of the DEP voltage V. The stiffness increase is quadratic with the applied electric potential (fitted, solid lines). Confinement strength can be as large as 0.85 pN/μm for 100 nm sized dielectric PS beads. In this case, the corresponding roll-off frequency is $f_T = 67.5$ Hz. (B, C, D) Hydrodynamic radius and surface conductivity σ_p for PS beads, CPNs and adenoviruses, respectively, confined and measured by the DEP trap at different DEP strengths. The hydrodynamic radius is independent of the applied potential and averages (solid lines) to be $r = 51.3 \pm 12.4$ nm, 45 ± 11.7 nm and 36.1 ± 7.1 nm for PS beads, CPNs and adenoviruses, respectively. The associated surface conductivities σ_p (red points) show little dependence on the applied potential. The conductivity values are $\sigma_p = 0.15 \pm 0.04$ S/m, $\sigma_p = 0.14 \pm 0.06$ S/m and $\sigma_p = 0.15 \pm 0.04$ S/m for PS beads, CPNs and adenoviruses, respectively. All error bars represent the experimental uncertainties at a 95% confidence interval (2 standard deviations) for a collection of particles at a given voltage V. Typically, the number of points N at $V = 1.6$ V is: $N = 79, N = 40$ and $N = 13$ for PS beads, CPNs and adenoviruses, respectively.